

Angular momentum transport and evolution of lopsided galaxies

Kanak Saha^{1*}, & Chanda J. Jog²

1. *Inter-University Centre for Astronomy and Astrophysics, Pune 411007, India*

2. *Department of Physics, Indian Institute of Science, Bangalore 560012, India*

Accepted xxxx Month xx. Received xxxx Month xx; in original form 9 September 2021

ABSTRACT

The surface brightness distribution in the majority of stellar galactic discs falls off exponentially. Often what lies beyond such a stellar disc is the neutral hydrogen gas whose distribution also follows a nearly exponential profile at least for a number of nearby disc galaxies. Both the stars and gas are commonly known to host lopsided asymmetry especially in the outer parts of a galaxy. The role of such asymmetry in the dynamical evolution of a galaxy has not been explored so far.

Following Lindblad’s original idea of kinematic density waves, we show that the outer part of an exponential disc is ideally suitable for hosting lopsided asymmetry. Further, we compute the transport of angular momentum in the combined stars and gas disc embedded in a dark matter halo. We show that in a pure star and gas disc, there is a transition point where the free precession frequency of a lopsided mode, $\Omega - \kappa$, changes from retrograde to prograde and this in turn reverses the direction of angular momentum flow in the disc leading to an unphysical behaviour. We show that this problem is overcome in the presence of a dark matter halo, which sets the angular momentum flow outwards as required for disc evolution, provided the lopsidedness is leading in nature. This, plus the well-known angular momentum transport in the inner parts due to spiral arms, can facilitate an inflow of gas from outside perhaps through the cosmic filaments.

Key words: galaxies: structure – galaxies: kinematics and dynamics – galaxies: spiral – galaxies: evolution – galaxies: halos

1 INTRODUCTION

With the expansion of the universe, the frequency of violent events such as interaction and mergers are expected to diminish leaving a galaxy nearly isolated. The evolution of such galaxies is mainly dependent on the internal processes which are generally slow with a typical time scale of a billion year. These slow internal processes which are believed to be the dominant mechanism of evolution in the later quiescent phase of galaxy evolution, are better known as the cause of secular evolution (Kormendy & Kennicutt 2004). Various non-axisymmetric features such as bars, spiral arms ($m = 2$ perturbation) are the commonly recognized driver of this evolution. As shown by the pioneering work of Lynden-Bell & Kalnajs (1972), spiral arms are able to lead the secular evolution via redistributing energy and angular momentum within the galaxy such that they eventually manage to enhance the central concentra-

tion as observations indicate (Pfenniger & Norman 1990; Zhang 1999; Laurikainen et al. 2007; Kormendy 2008). An important outcome of Lynden-Bell & Kalnajs (1972) paper is that in order to drive the evolution in the right direction (i.e., by angular momentum flowing outward), the spiral arms have to be trailing a fact that was difficult to be determined by the observations at the time. The role of bars too are now well established in this context. Bars are known to grow via transferring angular momentum outward and eventually goes through the buckling instability to form a boxy/peanut bulges (Combes et al. 1990; Raha et al. 1991; Athanassoula & Misiriotis 2002; Debattista et al. 2004; Saha et al. 2010; Saha & Naab 2013). Apart from hosting spiral arms and bars, many disc galaxies are also lopsided ($m = 1$ perturbation) and generally the asymmetry is prominent in the outer parts of the galaxy. However, the precise role of lopsided asymmetry in driving the evolution in galaxies has been little explored.

Indeed, more than a third of the spiral galaxies host large-scale lopsided asymmetry (Richter & Sancisi 1994;

* E-mail:kanak@iucaa.ernet.in

Rix & Zaritsky 1995; Bournaud et al. 2005; Zaritsky et al. 2013), see Jog & Combes (2009), for a discussion of the threshold of lopsidedness. Some of the mechanisms that are shown to generate lopsidedness in the outer galaxy are: cooperation of orbital streams to a lopsided pattern (Earn & Lynden-Bell 1996); response of an axisymmetric disc to a lopsided dark halo (Jog 1997, 1999); satellite infall onto a galaxy (Zaritsky & Rix 1997); a tidal encounter (Bournaud et al. 2005; Mapelli et al. 2008); asymmetric gas accretion (Bournaud et al. 2005) or through internal disc instabilities (Saha et al. 2007; Dury et al. 2008). No unique mechanism for generating lopsidedness has been identified so far, and it could well be that a combination of different processes is at work. Further, it has been shown that for isolated galaxies, the amplitude of lopsidedness is uncorrelated with the strength of tidal interaction (Bournaud et al. 2005; van Eymeren et al. 2011a) or the presence of nearby companions (Wilcots & Prescott 2004). Whatever might be the origin, both the stellar distribution (Block et al. 1994; Rix & Zaritsky 1995; Bournaud et al. 2005) and the neutral hydrogen gas distribution in the outer parts (Baldwin et al. 1980; Richter & Sancisi 1994; Angiras et al. 2006, 2007; van Eymeren et al. 2011a,b) of a galaxy are known to be lopsided. The strength of lopsidedness, as measured by the fractional Fourier amplitude of the $m = 1$ component is, on average, comparable to that of the $m = 2$ component as seen in spiral structure and bars (Jog & Combes 2009). Despite this, surprisingly, the dynamical effects of lopsidedness on galaxy dynamics and evolution have not received much attention. Being a prominent asymmetry in the outer parts, lopsidedness can produce torque the way bars and spirals do in the inner regions, and redistribute angular momentum in the galaxy. But the direction and detailed mechanism of this angular momentum transport has not been studied yet in detail, and we note that it will depend crucially on several factors such the underlying mass distribution, pattern speed, and overall whether the lopsidedness is trailing or leading.

Determining the sense of rotation in a galaxy has been a long-standing challenge (e.g., Pasha & Tsitsin 1979). The spiral arms ($m = 2$) are typically believed to be trailing on theoretical grounds because this facilitates outward transport of angular momentum (Lynden-Bell & Kalnajs 1972) and very recently ALMA shows clear evidence of a trailing spiral feeding the Seyfert 1 nucleus in NGC 1566 (Combes et al. 2014). On the other hand, in the case of a lopsided ($m = 1$) mode, when the sense of rotation can be determined at all, it seems to be leading, that too in the inner parts as in M31 (Considered & Athanassoula 1982). In ESO 297-27, the inner single arm leads while an outer three arms are trailing (Grouchy et al. 2008). There is also the reverse case when the outer two-armed pattern leads while the inner one-arm trails as in NGC 4622 (Buta et al. 2003). Thus while there is some evidence for lopsidedness being leading in the inner parts, it needs to be confirmed whether it is leading or trailing in the outer parts.

The current paper focuses on the issue of angular momentum flow due to a lopsided perturbation in a disc galaxy. We follow the treatment of Lynden-Bell & Kalnajs (1972); Goldreich & Tremaine (1979); Binney & Tremaine (2008) to derive the total torque which is a sum of gravity torque and advective torque (also known as Lorry transport as

dubbed by Lynden-Bell & Kalnajs (1972)) imparted by a lopsided perturbation on the outer disc. We show that angular momentum flow in a pure exponential disc gives rise to unphysical result, namely that the sign of angular momentum flow changes abruptly at a transition point which corresponds to the point where $\Omega - \kappa$, the kinematic precession frequency of a lopsided mode changes from being retrograde to prograde. However, the inclusion of a dark matter halo sets the angular momentum flow in the outward direction as necessary for disc evolution, provided lopsidedness is leading in nature.

The paper is organized in the following way. Section 2 describes the primary model for the disc and halo that we consider. Section 3 contains the calculation of the dispersion relation for the lopsided modes. The basic calculation of torque and hence the angular momentum transport (hereafter AMT) due to a lopsided perturbation are presented in section 4. Section 5 contains results and Section 6 contains discussion. The primary conclusions drawn from this work are presented in section 7. The appendix contains calculation and handy formula for obtaining different disc frequencies for various mass distribution.

2 DISC AND HALO MODEL

We consider three components to model a typical nearby disc galaxy namely stars, neutral gas and dark matter. For each of these components, analytic density profiles are employed to obtain the potential and other dynamical parameters. The galactic cylindrical co-ordinates R, φ, z are used throughout.

The density distribution of stars in our model galaxy follows an exponential fall-off with central surface density Σ_{s0} and a scale length R_d as (Freeman 1970)

$$\Sigma_s(R) = \Sigma_{s0} e^{-R/R_d}. \quad (1)$$

Motivated by the findings of Bigiel & Blitz (2012), we use the following exponential distribution as seen in a number of nearby disc galaxies

$$\Sigma_g(R) = \Sigma_{g0} e^{-1.65 \times R/R_{25}}, \quad (2)$$

where the fitted central gas surface density $\Sigma_{g0} = 28.2 M_\odot \text{pc}^{-2}$ according to Bigiel & Blitz (2012) and R_{25} denotes the radius where the B-band surface brightness drops to 25 mag arcsec $^{-2}$. We use a different value for Σ_{g0} as mentioned below.

Then net surface density in the disc is given by

$$\Sigma_0(R) = \Sigma_s(R) + \Sigma_g(R),$$

and as shown in Fig. 1.

The expression for the potential and epicyclic frequencies can be found in Binney & Tremaine (2008). The general expression for an epicyclic frequency in terms of the potential Ψ is given as

$$\kappa^2 = \left[\frac{\partial^2 \Psi}{\partial R^2} + \frac{3}{R} \frac{\partial \Psi}{\partial R} \right]_{z=0} \quad (3)$$

For an exponential disc, the potential at the mid-plane is given as

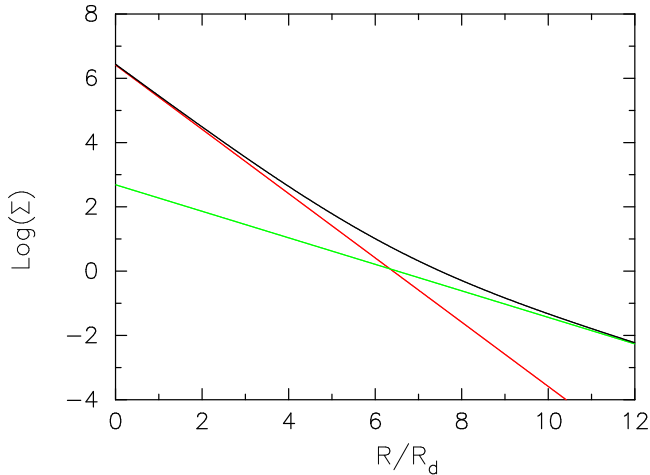


Figure 1. Exponential surface density distribution for the stars and gas. The red curve denotes stars, green one for the gas. The total surface density is denoted by the solid black line. The parameters used are given in section 2. The unit of surface density is in $M_{\odot} \text{pc}^{-2}$.

$$\Psi_s(R, 0) = -\pi G \Sigma_{s0} R [I_0(y) K_1(y) - I_1(y) K_0(y)], \quad (4)$$

where $y = R/2R_d$; I_0 , I_1 and K_0 , K_1 are the modified Bessel functions of first and second kind respectively. Then the epicyclic frequency is obtained to be

$$\kappa_{disc}^2 = \frac{\pi G \Sigma_{s0}}{R_d} [4I_0 K_0 - 2I_1 K_1 + 2y(I_1 K_0 - I_0 K_1)] \quad (5)$$

Similarly, the relevant potential and epicyclic frequency for the gas component are derived.

The dark matter halos is modelled as an axisymmetric pseudo-isothermal halo with a density distribution given by (de Zeeuw & Pfenniger 1988)

$$\rho_{dm}(R, z) = \frac{\rho_0}{1 + \frac{S_a^2}{R_c^2}}, \quad (6)$$

where $S_a^2 = R^2 + z^2/q^2$, q denotes flattening or the ratio of the vertical to planar axes and ρ_0 is the central density and R_c is the core radius. The corresponding potential in the spherical co-ordinates is obtained by solving the Poisson equation. This is then written in the cylindrical co-ordinates and from this an expression for κ_{halo} is obtained using the general definition for the epicyclic frequency given in Eq. [3].

In order to keep it simple and highlight the primary results from this work, we restrict ourselves to a particular model for which we have presented all the calculations here. For the stars, we have used $\Sigma_{s0} = 610.3 M_{\odot} \text{pc}^{-2}$ and $R_d = 3 \text{ kpc}$ – implying a total stellar mass ($M_d = 2\pi \Sigma_{s0} R_d^2$) of $3.45 \times 10^{10} M_{\odot}$.

For the gas distribution, we use $\Sigma_{g0} = 14.7 M_{\odot} \text{pc}^{-2}$ and $R_{25} = 4R_d$ which gives a total gas mass (M_g) in the model as $4.88 \times 10^9 M_{\odot}$ which is about 14% of the stellar mass (i.e., $M_g = 0.14M_d$). The reason for choosing a lower value for the Σ_{g0} is that we wanted the total gas mass to be less than $\sim 20\%$ of the chosen total stellar mass so that the disc does not go unstable. However, since we are not worrying about the stability of the total disc, these values

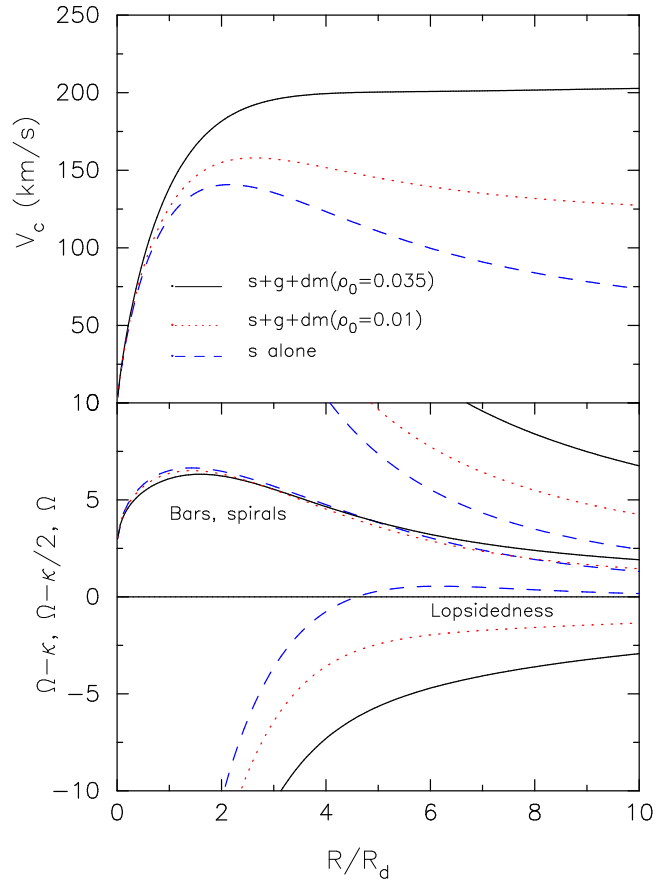


Figure 2. The upper panel showing the total circular velocity curves for two different models of stars+gas+dark matter and one with stars alone (shown for comparison). In the lower panel, we show their corresponding frequency profiles: circular frequency Ω (top 3 curves), $\Omega - \kappa/2$ for $m=2$ (middle 3 curves) and $\Omega - \kappa$ for the slow $m=1$ mode (bottom 3 curves). The frequencies are in units of $\text{kms}^{-1} \text{kpc}^{-1}$.

are arbitrary at the moment but agree with the range of typical values seen in a galaxy.

The flattening and core radius of the dark matter halo are fixed at $q = 0.9$ (considered to be nearly spherical, for simplicity) and $R_c = 1.65R_d$; the central density $\rho_0 = 0.035 M_{\odot} \text{pc}^{-3}$. The circular velocity curve for this stars+gas+dark matter halo configuration is shown in the upper panel (solid black line) of Fig 2. In order to have a falling rotation curve and study its effect on the kinematic description of lopsidedness, we have made minimal changes in the halo configuration e.g., decreased ρ_0 to $0.01 M_{\odot} \text{pc}^{-3}$ (roughly by a factor of 3); the corresponding circular velocity is shown by the dotted line in the upper panel of Fig 2. The falling rotation curve we have considered (with a gradual fall of 30 kms^{-1} over 30 kpc) is reasonable - e.g., our own Galaxy shows this (Brand & Blitz 1993) which also helps explaining the high amplitude of HI flaring seen in the outer parts (Saha et al. 2009). The lower panel of Fig. 2 will be explained in Section 3.

3 KINEMATIC LOPSIDEDNESS AND DISPERSION RELATION

We consider both the stellar and gas disc initially axisymmetric and embedded in an axisymmetric oblate dark matter halo whose density distribution are as mentioned in previous section. We treat both the stellar and gas disc in the outer part of a galaxy as cold self-gravitating fluid disc with velocity dispersion (σ) being much less than the local circular velocity (V_c) i.e., $\sigma/V_c \ll 1$. When such a disc is subject to a lopsided ($m = 1$) perturbation of the form $\sim \cos(\varphi - \omega t)$, we can write the density, potential and velocities in the galactic plane as

$$\begin{aligned}\Sigma(R, \varphi, t) &= \Sigma_0(R) + \Sigma'(R, \varphi, t) \\ \Psi(R, \varphi, t) &= \Psi_0(R) + \Psi'(R, \varphi, t) \\ v_R(R, \varphi, t) &= 0 + v'_R(R, \varphi, t) \\ v_\varphi(R, \varphi, t) &= R\Omega(R) + v'_\varphi(R, \varphi, t),\end{aligned}$$

Here the circular frequency $\Omega = V_c/R$ and the perturbed surface density and potential are connected via the Poisson equation as

$$\nabla^2 \Psi' = 4\pi G \Sigma' \delta(z) \quad (7)$$

Then the linearized equations of hydrodynamics namely the Euler and continuity equations can be written as:

$$\frac{Dv'_R}{Dt} - 2\Omega v'_\varphi = -\frac{\partial \Psi'}{\partial R} - \frac{1}{\Sigma_0} \frac{\partial P'}{\partial R} \quad (8)$$

$$\frac{Dv'_\varphi}{Dt} + \frac{\kappa^2}{2\Omega} v'_R = -\frac{1}{r} \frac{\partial \Psi'}{\partial \varphi} - \frac{1}{R\Sigma_0} \frac{\partial P'}{\partial \varphi} \quad (9)$$

$$\frac{D\Sigma'}{Dt} + \frac{1}{R} \frac{\partial(R\Sigma_0 v'_R)}{\partial R} + \frac{\Sigma_0}{R} \frac{\partial v'_\varphi}{\partial \varphi} = 0 \quad (10)$$

In the above equations $D/Dt \equiv \partial/\partial t + \Omega \partial/\partial \varphi$ and κ is the epicyclic frequency in the disc. For a stellar fluid, the self-consistent derivation of anisotropic stress tensor can be done only for special cases, because of the closure problem (Binney & Tremaine 2008). Although Hunter (1979) derived a set of dynamical equations for the anisotropic pressure assuming circular motions, a general solution and interpretation remained unclear. For our calculation, we consider a polytropic equation of state, $P = \sigma^2 \Sigma^\gamma$, with $\gamma = 1$ (also called an isothermal equation of state) and $\sigma^2 = (\frac{dP}{d\Sigma})|_{\Sigma_0}$ constant throughout the disc (Binney & Tremaine 2008). This is a good approximation for the gas disc where various observations indeed indicate that the gas velocity dispersion remains nearly constant with radius and does not depend on the local unperturbed mass density (Spitzer 1978; Malhotra 1995; Lewis 1984) but not for the stars which are better described by a polytropic index $\gamma = 2$ (Kikuchi et al. 1997). Since lopsidedness is mostly prominent in the outer parts of a galaxy where stellar density drops down significantly (so does the velocity dispersion as $\sigma^2 \propto \Sigma$), we, to a zeroth order approximation, applied the same isothermal equation of state to describe both the components. We shall discuss the impact of this simplified assumption on the angular momentum transport in the following section.

Then writing the perturbed variables in terms of Fourier transform as $X'(R, \varphi, t) = \Re(X_a(R)e^{i(\varphi - \omega t)})$ and substituting them back in the equations of motion, the perturbed

planar velocity field (i.e., radial and azimuthal) can be written in a compact form:

$$\bar{v}_a = A\bar{\chi}_a, \quad (11)$$

with $\bar{v}_a = \begin{bmatrix} v_{Ra} \\ v_{\varphi a} \end{bmatrix}$ and $\bar{\chi}_a = \begin{bmatrix} \frac{d\Psi_{ha}/dR}{D_1} \\ \frac{\Psi_{ha}/R}{D_1} \end{bmatrix}$ and the matrix A is given by,

$$A = \begin{bmatrix} i(\omega - \Omega) & -i2\Omega \\ \frac{\kappa^2}{2\Omega} & -(\omega - \Omega) \end{bmatrix} \quad (12)$$

In the above equations,

$$D_1 = -i \det(A) = \kappa^2 - (\omega - \Omega)^2,$$

and

$$\Psi_{ha} = \Psi_a + \sigma^2 \frac{\Sigma_a}{\Sigma_0}.$$

Then writing the radial part of the perturbed quantities as $X_a(R) = \Re X_a e^{-i\Phi_p(R)}$, with Φ_p being the phase and using a WKB approximation (Binney & Tremaine 2008), we have the following dispersion relation for $m = 1$ lopsided perturbation

$$D_1 - 2\pi G \Sigma_0(R) |k| + \sigma^2 k^2 = 0, \quad (13)$$

where the wavenumber $k = -d\Phi_p(R)/dR$.

For trailing perturbation $d\Phi_p(R)/dR < 0$, while it is positive for a leading case. Note that the general form of the dispersion relation remains unchanged for any fluid described by a polytropic equation of state except the fact that the velocity dispersion depends on the local surface density and polytropic index (as discussed above). The dispersion relation will be useful later in deriving angular momentum transport under the WKB limit. In absence of self-gravity and pressure of the perturbation, the slow $m=1$ lopsided pattern would precess with a frequency $\Omega_{pf} = \Omega - \kappa$. In Fig. 2, we show the free precession frequencies for $m = 1$ and $m = 2$ perturbations in a cold exponential disc. It was Lindblad who first showed (e.g., Binney & Tremaine 1987) that for an $m = 2$ spiral arm to survive in a disc with strong differential shear, the radial variation of $\Omega - \kappa/2$ should be nearly zero and this condition is nearly satisfied in the region around the peak of this curve (see Fig. 2). In fact, in most spiral galaxies, the spiral arms are contained within the inner parts of the optical radius or about two disc scale lengths, taking the optical disc to be about 4 – 5 disc scale lengths (Binney & Merrifield 1998).

We employ a similar analogy to suggest that lopsidedness should be preferentially seen in the outer parts of a galaxy. For the exponential disc, the differential precession i.e., the value of radial derivative of $\Omega - \kappa$, rapidly increases below 4 scale lengths. However, beyond this radius, the radial variation of $\Omega - \kappa$ flattens out and becomes almost close to zero. This turns out to be an ideal situation for the $m = 1$ lopsidedness to naturally avoid the differential shear. In general, a naturally favourable situation for the lopsidedness to survive would be where the circular velocity falls as one goes outwards. This occurs in a Keplerian case as in a

disc around the central black hole, this case will be studied in a future paper.

But lopsidedness is observed in galaxies with a flat rotation curve too. For a flat rotation curve, $\kappa = \sqrt{2}\Omega$ and the pattern frequency becomes $\Omega_{pf} = -0.414\Omega$ in which case, the differential shear becomes non-zero. Then inclusion of self-gravity helps as shown previously by Saha et al. (2007). Basically, self-gravity tries to reduce the radial epicyclic frequency κ so that there is a net reduction in the radial variation of Ω_{pf} . The situation gets more favourable when the net circular velocity falls off moderately in the outer parts and one such case is shown in Fig. 2 in which case the differential precession is much lower compared to the galaxies with flat rotation curve. However, even with the inclusion of global self-gravity, the preferred region for lopsidedness seems to be the outer parts of a disc, as the differential shear in the inner region is too strong (Saha et al. 2007). There is another physical reason for lopsidedness to be seen mainly in the outer region since the self-gravity of the disc resists any distortion of type $m = 1$ inside of about 2 disc scale lengths (Jog 1999, Jog 2000) as shown by a self-consistent disc response to an imposed potential.

The exponential disc by itself can support kinematical lopsidedness for a long time as seen from the near constancy of $\Omega - \kappa$ (Fig. 2). While addition of the dark matter halo changes this constancy such a way that the disc plus halo system is not so supportive of the $m = 1$ mode (unless the halo is such that the overall rotation curve is falling in nature). On the other hand, the inclusion of the dark matter halo makes it possible to allow a smooth outward transport of angular momentum without any radial break and hence is a dynamically preferred state as shown in the subsequent section.

4 ANGULAR MOMENTUM TRANSPORT DUE TO A LOSPDED PATTERN

In the following, we compute the torque due to a lopsided perturbation imposed onto the disc. We assume that the lopsided perturbation is stationary and not growing. The disc has no net inflow/outflow of matter from outside/inside i.e., mass conservation is strictly followed. In addition, we assume that the dark matter particles do not take part in the angular momentum transport i.e., these particles neither gain nor lose angular momentum; the halo is considered here as a simple potential bath.

4.1 Gravity transport

Following Lynden-Bell & Kalnajs (1972), we write the torque exerted by an $m = 1$ lopsided perturbation on the disc material outside a given radius R_a as

$$C_{grav}(R_a) = \frac{1}{4\pi G} \int_{-\infty}^{\infty} \int_0^{2\pi} R \frac{\partial \Psi'}{\partial R} \frac{1}{R} \frac{\partial \Psi'}{\partial \varphi} \Big|_{R=R_a} R d\varphi dz. \quad (14)$$

Note that the above integrand is second order in perturbed quantities. There is no torque on the disc to first order.

We evaluate the gravitational torque in the WKB limit (using tightly wrapped potential perturbation) with Ψ' given

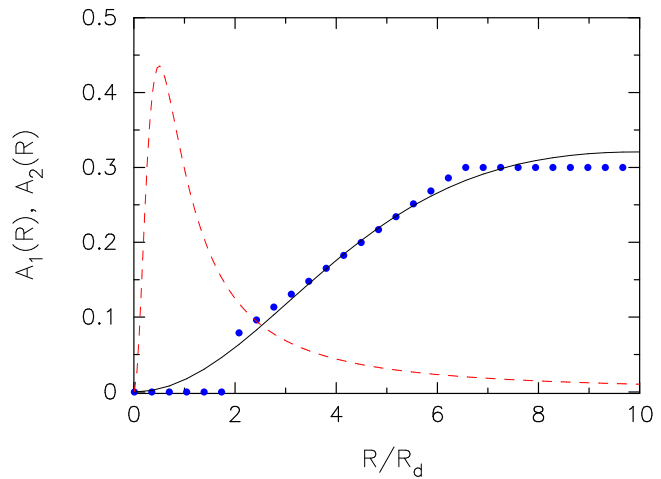


Figure 3. Model radial profiles for the $m = 1$ lopsided perturbation $A_1(R)$ and the $m = 2$ perturbation, $A_2(R)$. The filled blue circles and solid line represent model 1 and model 2 for the lopsidedness (see Eq. 28). Whereas, the dashed red line for A_2 as given in Eq. 29.

by

$$\Psi'(R, \varphi, 0) = \Psi_a(R) e^{i[\varphi - \Phi_p(R)]}$$

Then the resulting expression for the torque is given by

$$C_{grav}(R_a) = \frac{1}{4} \frac{R_a |\Psi_a(R_a)|^2}{G} \frac{k}{|k'|}, \quad (15)$$

Where

$$k' = \sqrt{k^2 + \frac{1}{R_a^2}}$$

At large distances from the centre of a disc i.e., in the outer parts $k' \simeq k$. Note that the gravity transport of angular momentum depends primarily on the square of the perturbing potential and sign of the phase variation of the perturbation. As is well known, only the trailing spiral ($k > 0$) (or any m-fold non-axisymmetric perturbation) can exert positive torque on the outer parts and transport angular momentum outward. The same is, of course, true for the $m=1$ lopsided perturbation i.e., the gravity torque due to a trailing lopsided perturbation induces outward transport of angular momentum. However, gravity torque alone does not tell the full story of angular momentum flow in galaxies. Below we discuss another mechanism of angular momentum transport proposed by Lynden-Bell & Kalnajs (1972).

4.2 Lorry transport

It has been shown that in the presence of a steady non-axisymmetric perturbation, stars away from resonances neither gain nor lose angular momentum. But these stars nevertheless help transporting angular momentum just as a system of lorries - a mechanism worked out by Lynden-Bell & Kalnajs (1972) who named it the "Lorry transport". According to them, in the presence of a trailing perturbation, stars with very small eccentricities gain angular momentum near their apocenters and lose it all near

their pericenters. In this sense, lorry transport of angular momentum by such stars opposes gravity transport of angular momentum. However, the net advective flux of angular momentum can have either sign when derived over a distribution of stars. Now, the total advective torque due to a lopsided perturbation can be calculated either following the original derivation of Lynden-Bell & Kalnajs (1972) or using the fluid equations following Goldreich & Tremaine (1979); Binney & Tremaine (2008) which we intend to use in the present paper. In this section, we calculate the advective torque in both ways and show under what condition they are equivalent.

Considering a simple two-integral distribution function (DF), the advective torque due to $m = 1$ perturbation can be written as (Lynden-Bell & Kalnajs 1972):

$$C_{adv}^{LBK} = -\frac{\pi R_a \Sigma_0 |\Psi_a|^2}{2 (\kappa a_0)^2} \frac{\partial}{\partial k} \sum_{l=-\infty}^{\infty} \frac{l \kappa I_l(k'^2 a_0^2)}{l \kappa + \Omega - \Omega_p}, \quad (16)$$

where R_a is a given radius within which we calculate the torque, a_0 is the average epicyclic amplitude with $J_1 = \kappa a_0^2$ denoting the average epicyclic energy. Then writing $\nu = (\Omega - \Omega_p)/\kappa$, where Ω_p is the pattern speed of a lopsided mode and using the properties of modified Bessel function, we have

$$C_{adv}^{LBK} = -\frac{2\pi \Sigma_0 k R_a |\Psi_a|^2}{\kappa^2} \sum_{l=1}^{\infty} \frac{I_{l-1}(k'^2 a_0^2) - l/k'^2 a_0^2 I_l(k'^2 a_0^2)}{1 - \nu^2/l^2}. \quad (17)$$

In the longwave limit $k' a_0 < 1$, the dominant contribution comes from the $l = 1$ term and in that case it can be shown that the advective torque is given by a rather simple formula:

$$C_{adv}^{LBK} = -\frac{R_a |\Psi_a|^2}{G} \frac{\pi G \Sigma_0 k}{\kappa^2} \frac{1}{1 - \nu^2}. \quad (18)$$

Note that the original derivation for the advective torque by (Lynden-Bell & Kalnajs 1972) has a typographical error; in that the term $1 - \nu^2$ should be in the denominator as it is in eq. 18 (Lynden-Bell 2014, private communication).

Now, we shall derive the advective torque under the fluid approximation. We begin by writing

$$C_{adv}^{FL}(R_a) = R_a^2 \int_0^{2\pi} d\varphi \Sigma_0 v'_\varphi v'_R \quad (19)$$

Note that the net torque is again second order in perturbed quantities. Substituting the perturbed velocities and carrying out the φ -integral, we have

$$C_{adv}^{FL}(R_a) = \frac{\pi}{2} \Sigma_0 R_a^2 (v_{R_a} v_\varphi^\dagger + v_{R_a}^\dagger v_\varphi), \quad (20)$$

† sign indicates the complex conjugate. Substituting v_{R_a} and $v_{\varphi a}$ from Eq. 11, we obtain

$$C_{adv}^{FL}(R_a) = -\frac{\pi \Sigma_0 k R_a}{D_1} \Psi_{ha}^2, \quad (21)$$

where D_1 is defined in section 3. Further using the WKB solution for a tightly wrapped lopsided density perturbation,

$$\Psi_{ha} = \left(1 - \frac{\sigma^2 |k|}{2\pi G \Sigma_0}\right) \Psi_a \quad (22)$$

Substituting the above in eq. 21 and using $D_1 = \kappa^2(1 - \nu^2)$ which we shall use interchangeably, it is possible to write the advective torque in a more familiar form:

$$C_{adv}^{FL}(R_a) = -\frac{R_a |\Psi_a|^2}{G} \frac{\pi G \Sigma_0 k}{\kappa^2} \frac{(1 - \frac{\sigma^2 |k|}{2\pi G \Sigma_0})^2}{1 - \nu^2} \quad (23)$$

Note that in the limit $\sigma \rightarrow 0$, we have

$$C_{adv}^{FL}(R_a) = C_{adv}^{LBK}(R_a) \quad (24)$$

The above equality which holds in the limit $\sigma \rightarrow 0$ implies that we basically have a pressure-less stellar fluid. The two-integral DF assumed by Lynden-Bell & Kalnajs (1972) also amounts to saying that the stars in epicyclic motion form a pressure-less cold self-gravitating system. From now on, we shall use eq. 23 to further deduce the value of advective torque. Utilizing the dispersion relation given by eq. 13, we can write eq. 23 as

$$C_{adv}^{FL}(R_a) = -\text{sign}(k) \frac{R_a |\Psi_a|^2}{4G} \frac{\kappa^2 (1 - \nu^2)}{\pi G \Sigma_0 |k|} \quad (25)$$

Eq. 25 is worth examining. Apart from the wavelength of the perturbation, it depends on the underlying mass distribution and the perturbing potential. In general, for a disc galaxy we have the inequality $\Omega \leq \kappa \leq 2\Omega$ satisfied over a wide range of potential variation from $\Psi_0 \sim 1/r$ to $\Psi_0 \sim r^2$ respectively. Then it follows in a straightforward way that for a general galactic potential, in the presence of any m -fold slowly rotating non-axisymmetric perturbation with $m \geq 2$, $D_m < 0$ within the disc, where $D_m = \kappa^2 - m^2(\Omega - \Omega_p)^2$. This holds true as well for a wide range of self-gravitating astrophysical discs as $\kappa^2 < m^2 \Omega^2$ always with $m \geq 2$. However, the scenario changes for $m = 1$; in which case, one could, in principle, have either situation i.e., $\kappa^2 > \Omega^2$ or $\kappa^2 < \Omega^2$. As we discuss in detail in Section 5, the exponential discs in galaxies happen to manifest this intriguing situation. This has far-reaching consequences for the dynamical evolution of galaxies as shown here.

4.3 Net AM transport

The net rate of change of angular momentum within the disc is obtained by combining the contribution from both the gravity torque and advective torque as

$$\frac{dL_z}{dt}(R_a) = -\text{sign}(k) \frac{R_a |\Psi_a|^2}{4G} \left[\frac{|k|}{|k'|} - \frac{\kappa^2 (1 - \nu^2)}{\pi G \Sigma_0 |k|} \right] \quad (26)$$

Substituting the perturbing potential by the perturbed surface density and using the fact that $\Sigma_a(R) = \Sigma_0(R) A_1(R)$, where $A_1(R)$ denotes the radial variation of lopsidedness in the disc (can be obtained via Fourier decomposition), we can write:

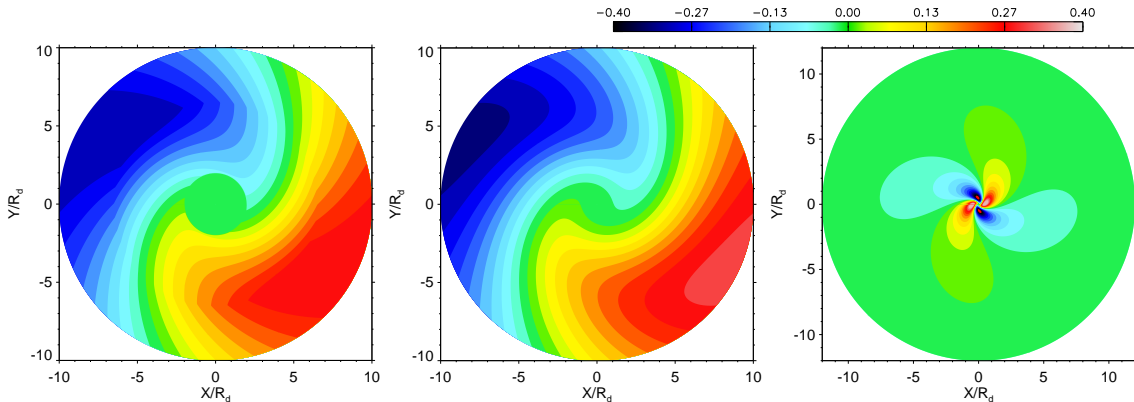


Figure 4. Perturbed surface density maps for the chosen models. The left and middle panels represent $m = 1$ perturbation corresponding to model 1 and model 2 respectively (see Eq. 28). The panel on the right for $m = 2$ perturbation for which the radial profiles are given by Eq. 29. Numerical values for the used parameters are given in section 4.3. All three panels are scaled to the same color bar.

$$\frac{dL_z}{dt}(R_a) \simeq -\text{sign}(k) (\pi^2 G \Sigma_0^2 R_a^3) \times \tan^2 \alpha A_1^2(R_a) \left[\cos \alpha - \frac{D_1 / \Omega^2 R_a \tan \alpha}{\pi G \Sigma_0 / \Omega^2} \right] \quad (27)$$

Eq. 27 is our working formula to compute the angular momentum transport. Apparently, neither gravity torque nor advective torque explicitly depends on the velocity dispersion of the system as we have used the dispersion relation given by Eq. 13 to remove the explicit dependencies. However, the torque depends on the wavelength of the perturbation ($2\pi/|k|$) or the pitch angle (α) which are, of course, related to the velocity dispersion of the system. It is trivial to see that the net magnitude of torque will change by changing the pitch angle of the lopsided perturbation. But it is not clear what is the pitch angle for any lopsided perturbation; it does measure how tightly wrapped a lopsided perturbation is. For simplicity, we shall use $\alpha \simeq 45^\circ$ corresponding to a WKB limit of $|kR| \simeq 1$ which crudely represents a logarithmic variation of the phase angle. Although, this is really pushing the WKB limit to a stage where it is not valid any more, as is often said, it might nevertheless give a good insight into the problem.

In order to proceed further, we need to know the functional form of $A_1(r)$ in a galaxy. In principle, this should be derived self-consistently as one of the eigen modes of the set of hydrodynamic equations (Eq. 7 - Eq. 10) stated in section 3 - similar to the eigen modes (which broadly capture the radially increasing behaviour of lopsidedness) of Saha et al. (2007). Since the amplitude of a linear eigenmode is arbitrary, we decided to connect our angular momentum transport to observed lopsidedness in disc galaxies. Guided by various observations (Rix & Zaritsky 1995; van Eymeren et al. 2011b), we use the following radial profiles for the lopsidedness in the disc:

$$A_1(R) = \epsilon_1 \left(2 \frac{R}{R_d} - 1 \right) \quad 2. \leq R/R_d \leq 6.5 \quad (\text{model1}) \\ = A_{10} \frac{(R/R_d)^2}{(1 + \beta_1 (R/R_d)^2)^\gamma}, \quad (\text{model2}) \quad (28)$$

ϵ_1 is the halo perturbation parameter and the linearly ris-

ing part of A_1 arises as a result of self-consistent response of the disc to halo perturbation Jog (2000) – this we refer to as model 1, the first formula in Eq. 28. The radial profile of A_1 corresponding to model 1 uses $\epsilon_1 = 0.025$ and is shown in Fig. 3. The other functional form for A_1 (smooth radial variation) is chosen ad-hoc but motivated by typical observational behaviour of lopsidedness in galaxies – refer to as model 2, the second formula in Eq. 28. For model 2, we choose $A_{10} = 0.0166$, $\beta_1 = 0.02$ and $\gamma = 1.5$, so that the average value of A_1 in the range $4 - 6R_d$ are around 0.25 (see Fig. 3). By carefully choosing the free parameters, the same functional form can roughly capture the typical radial variation of $m = 2$ perturbation such as bars/spirals (e.g., see Durbala et al. 2009, for radial variation of A_2) and we write this as:

$$A_2(R) = A_{20} \frac{(R/R_d)^2}{(1 + \beta_2 (R/R_d)^2)^\gamma}, \quad (29)$$

where the free parameters $A_{20} = 7.5$, $\beta_2 = 5.0$ and $\gamma = 1.8$ gives rise to a radial profile for A_2 as shown in Fig. 3. The perturbed surface density maps corresponding to these A_1 and A_2 profiles are as shown in Fig. 4. One can, in principle, change these free parameters to model any other profiles for A_1 and A_2 . In the following, we shall employ these profiles for the calculation of total torque in the disc exerted by the lopsided perturbation and the $m = 2$ perturbation.

From eq. 27, it is obvious that in the absence of an advective torque, any m-fold trailing non-axisymmetric perturbation would transport angular momentum outward by gravity torque alone. When advective torque is added, the net sign of the angular momentum flow is not clear a priori; as mentioned elsewhere it can in some cases add on to the effect of the gravity torque or oppose it. One of the purposes of this paper is to explore the parameter space and various disc-halo configurations to understand the flow of angular momentum in disc galaxies - which, in turn, is crucial for understanding the evolution of galaxies. In the following section, we restrict ourselves to a slowly rotating lopsided perturbation and discuss briefly here the $m = 2$ case just for the purpose of illustration.

Fig. 5 shows the radial variation of torque in a pure

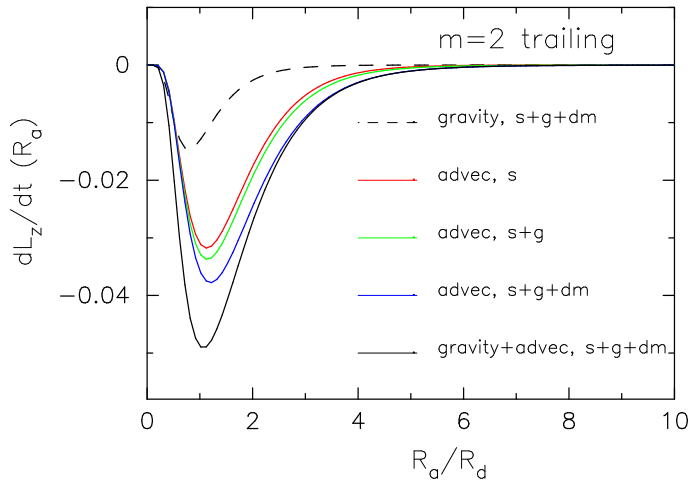


Figure 5. Radial variation of angular momentum flow in the disc for $m = 2$ trailing spiral. In the figure, 's' stands for stars, 'g' for gas and 'dm' for dark matter. Negative sign on $dL_z/dt(R_a)$ indicates that the disc within R_a loses angular momentum in the presence of an $m = 2$ trailing spiral. The unit of dL_z/dt is GM_d^2/R_d .

exponential disc, in disc with stars and gas, and in our full galaxy model, i.e., stars+gas+dark matter halo due to a tightly wrapped $m = 2$ perturbation. In all cases, the $m = 2$ perturbations (e.g., spiral arms) transfers angular momentum outwards when they are trailing ($k > 0$), a result well-known for the last four decades (Lynden-Bell & Kalnajs 1972) and very recently ALMA reveals the evidence of a trailing spiral carrying angular momentum outward in NGC 1566 (Combes et al. 2014). It is interesting to note that in the long-wave limit, the net torque (gravity+advective), calculated in our full model of stars+gas+dark matter, beats the gravity torque alone by a factor of ~ 3 depending on the amplitude of the $m = 2$ perturbation (a fact that had been suspected in the original paper by Lynden-Bell & Kalnajs (1972)). For stars alone disc, the magnitude of the advective torque is roughly a factor of 2 times more than the corresponding gravity torque. It is also worth to note that the advective torque supports the gravity torque in the presence of an $m = 2$ trailing spiral.

5 SLOWLY ROTATING LOSPISDED PATTERN

The pattern speed of a lopsided perturbation is an unknown quantity as there is no observational measurement attempted so far unlike the galactic bar (Jog 2011). In its absence, we assume a slowly rotating lopsided pattern imposed on the disc with $\Omega_p \ll \Omega$. An exponential stellar disc is shown to support lopsidedness as a discrete normal mode with such a small pattern speed and this has been further supported by N-body simulations (see Saha et al. 2007). However, for $m = 1$, one gets a peculiar situation, namely that if the pattern speed $\Omega_p > 0$, then there is no ILR (inner Lindblad resonance) as $\Omega - \kappa$ is negative, in general, for galaxies. On the other hand, an ILR can only exist for $\Omega_p < 0$ i.e., for a retrograde lopsided perturbation. But then there can be no corotation (Jog 2011) which might not turn out to be favourable for the lopsided perturbation. A

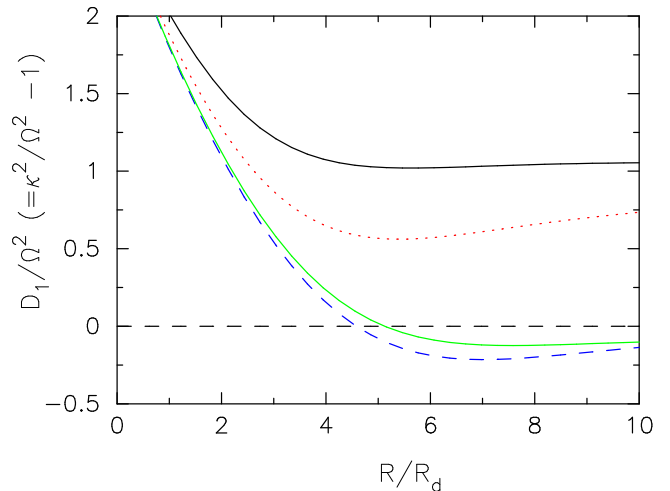


Figure 6. D_1/Ω^2 parameter versus radius for an exponential disc with stars-alone, stars+gas and stars+gas+dark matter halo. The star-alone disc and the stars plus gas disc show an "unphysical" situation, namely a change of sign in D_1/Ω^2 and hence the advective torque C_{adv} due to $m = 1$ perturbation (see subsequent figures). This problem is solved on addition of the dark matter halo where the mass builds up more gradually at large radii. The black solid and blue dashed lines represent stars+gas+dark matter ($\rho = 0.035$) and stars+gas+dark matter ($\rho = 0.01$) respectively.

galaxy can evolve without an ILR; in fact for certain non-axisymmetric perturbation (e.g., a bar or even lopsidedness) it can be a bonus. An absence of a strong ILR is desirable to complete the feedback loop required for the swing amplification (Toomre 1981) through which these perturbation might actually grow. So we consider a small prograde pattern speed for the lopsidedness so that the corotation is placed at very large radii in the disc.

In this limit, we have $D_1 \simeq \kappa^2 - \Omega^2$. In Fig. 6, we show that the radial variation of this parameter D_1 which appears to play a pivotal role in deciding the direction of angular momentum transfer due to advective mechanism in galaxies. It is clear from the figure that for a pure exponential disc, the parameter D_1 flips its sign from positive to negative at a radius of $4.6R_d$, which we call as the *transition radius*, denoted as R_{tr} . This transition corresponds to when κ the epicyclic frequency, falls below Ω the angular speed. For a self-gravitating disc, this may seem counter-intuitive since for most realistic rotation curves κ is $\geq \Omega$. However, such a situation can occur for example, for highly centrally concentrated (or super-Keplerian or steeper than Keplerian) mass distributions, including an exponential disc as shown here. Interestingly, a number of mass distributions such as the Toomre's model n, or a Gaussian density distribution, which are widely used in modelling astrophysical discs also possess a transition radius (R_{tr}). These cases are given in the Appendix, and their implications are discussed in section 6.

In Fig. 7 and Fig. 8, we show the angular momentum transport by the $m = 1$ lopsided perturbations as shown in Fig. 4, first, for an exponential disc distribution. As can be seen from these figures, the gravity torque alone is negative at all radii when the $m = 1$ lopsidedness is trailing. It is interesting to note that the advective torque is dominating the

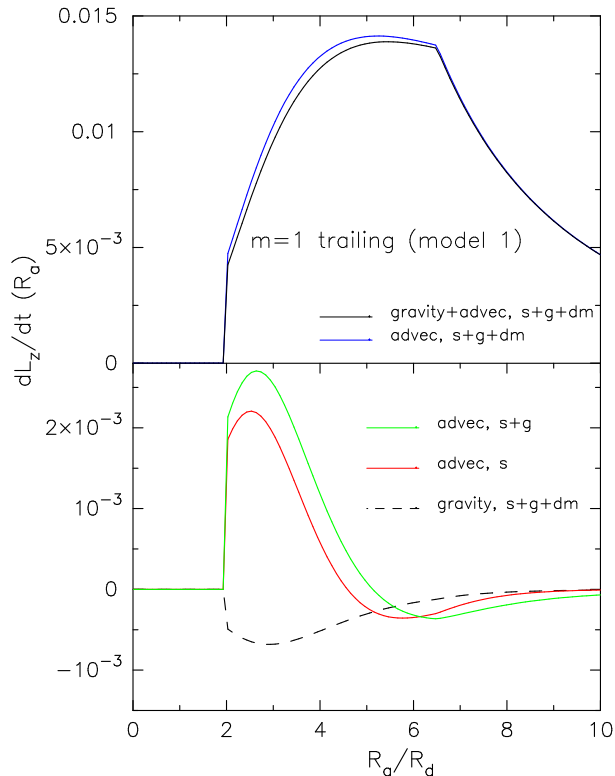


Figure 7. Radial variation of the torque i.e., the rate of change of angular momentum in the disc for an $m = 1$ trailing lopsidedness (model 1, corresponding to left panel of Fig. 4). Note that in the presence of a dark halo, the disc gains angular momentum (by advective transport) for a trailing $m = 1$ at all radii. The unit of dL_z/dt is given by GM_d^2/R_d .

gravity torque roughly by a factor of 2 and oppose the gravity torque (unlike the $m = 2$ trailing case). However, sign of the net torque (advective+gravity) flips exactly at the transition radius of the exponential disc. The presence of a transition point hampers the smooth angular momentum flow in the disc – irrespective of whether it is trailing or leading. This, in turn, might lead to an unfavourable situation for the evolution of galaxies. However, such a situation can only be completely eliminated if we add sufficient amount of gas in it and/or embedded the disc in a dark matter halo as discussed below.

5.1 Inclusion of gas and dark matter halo

If we include a reasonable amount of cold gas in the disc (say 10-15%) – as seen in late-type galaxies (e.g., Binney & Tremaine 1987), then the transition radius, R_{tr} , changes from $4.6R_d$ to about $5.1R_d$ (see Fig. 6). This is not because of any physical property such as dissipation related to the gas component per se but because of the gas distribution that is taken to fall slower than that of stellar distribution here as observed (see Eq. 2, Section 2). If we were to add more gas, say more than 20% by disc mass, then we do not have the transition radius any more in the disc. But gas fraction higher than 20% is not likely since that would make a disc highly unstable to the growth of gravitational instabilities (Jog 1996).

The transition point is also avoided when the disc is

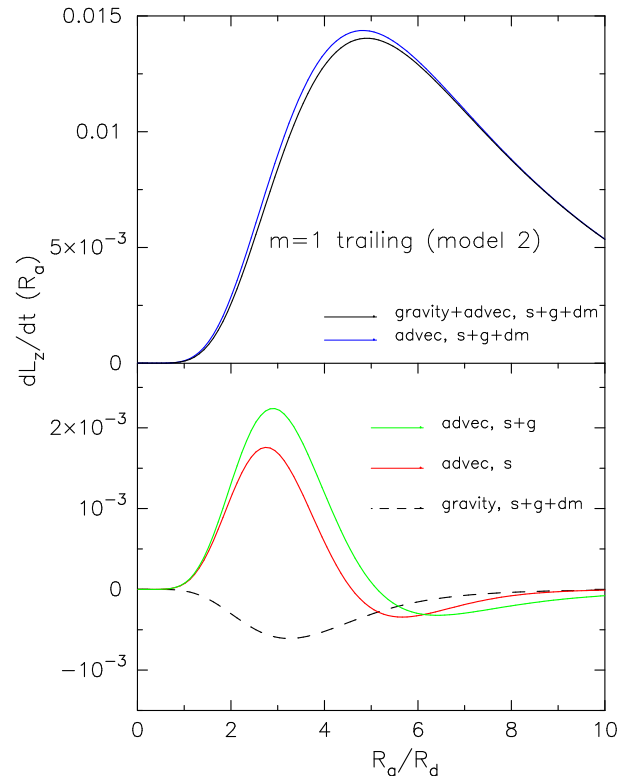


Figure 8. Same as in Fig. 7 but for model 2 corresponding to the middle panel of Fig. 4. Again due to advective transport, the disc gains angular momentum at all radii in the presence of a dark halo. The unit of dL_z/dt is given by GM_d^2/R_d .

embedded in a dark matter halo. In either case, the net κ exceeds Ω and hence the transition point is avoided (see Fig. 6). In the presence of a dark matter halo that gives rise to a flat rotation curve, we get $D_1 > 0$ at all radii (where V_c is constant corresponding to $\rho_0 = 0.035M_\odot pc^{-3}$); the same holds true even when the rotation curve is moderately falling (see Fig 2 and Fig. 6) which arises when use the other dark halo model with central density $\rho_0 = 0.01M_\odot pc^{-3}$. Adding some amount of gas makes D_1/Ω^2 to be slightly higher than 1 (for the case with V_c constant). These findings have significance for the slow evolution of galaxies as discussed next.

The net transfer of angular momentum due to an $m = 1$ trailing lopsided pattern in an exponential stellar disc with gas and our full model with the dark matter halo (with $\rho_0 = 0.035M_\odot pc^{-3}$) having a flat rotation curve are shown in Fig. 7 and Fig. 8. The lopsided perturbation used in deriving these figures are the same as in the first two panels of Fig. 4. As discussed below, the basic facts of angular momentum transfer do not change appreciably whether we use either models of $A_1(R)$. Both these figures indicate that the net transfer of angular momentum in the presence of a dark matter halo giving rise to a flat rotation curve is enhanced roughly by a factor of 7 over that due to stars+gas alone. Note that a dark matter halo explicitly affects the advective torque by changing the free precession frequency (Ω_{pf}) of the slow lopsided perturbation. Decreasing the amount of dark matter in the galaxy reduces the value of D_1 (see Fig. 6) and hence the net torque also reduces. In other words, in a disc galaxy with a falling rotation curve (in our case, one with $\rho_0 = 0.01M_\odot pc^{-3}$), the net outward flow of angular momen-

tum will be slower (approximately by a factor of 3 compared to the other dark halo producing the flat rotation curve) and the process will be slowest or inefficient in the limit where dark matter halo is totally absent. In such an extreme case, the disc alone is barely stable against local perturbations and a non-responsive dark matter halo is shown to be crucial to ensure local disc stability (Jog 2014) as well as to prevent global bar-like instability (Ostriker & Peebles 1973). The inclusion of a rigid dark matter halo in our picture has the effect that it removes the transition point in the galaxy and the total torque is positive at all radii for the trailing lopsided perturbations we consider here i.e., the disc within $R = R_a$ gains angular momentum. In other words, the inclusion of a reasonable dark matter halo reinforces the angular momentum to flow inwards if the lopsidedness is trailing. If this is allowed, such perturbation can not last long and can not drive the galaxy evolution. On the other hand, if galaxies are to evolve by maximizing entropy, the angular momentum has to be transferred outward – demanding that *lopsidedness has to be leading in nature*.

In Fig. 9, we show that indeed it is the leading lopsided perturbation which can drive the angular momentum flow outwards as the trailing $m = 2$ perturbation does, albeit less vigorously in the inner regions. Note that for $m = 2$, the final peak of the net AMT occurs approximately at a region where $A_2(R)$ has its maximum. This can be understood as follows: the second term for $m = 2$ in the square bracket in Eq.[27] is nearly flat in the inner few scale length followed by a gentle rise in the outer parts of the disc where A_2 falls sharply to zero – when multiplied the net peak is basically determined by the A_2 . For $m = 1$, the second term is a smoothly rising function right from the center and A_1 is also rising but reaching its peak after $6 R_d$ (see Fig. 3)– when multiplied the net peak occurs before $6 R_d$. In essence, the peak of AMT is basically determined by the radial variation of the perturbation and the second term in square bracket in eq. (27) which largely determines the advective transport. For the kind of perturbations (Fig. 4) we have used, the net torque due to the $m = 2$ trailing perturbation is an order of magnitude higher than $m = 1$ leading perturbation within 2 disc scale length. On the other hand, in the region beyond $\sim 4 - 6$ scale length, the torque due to the $m = 1$ leading perturbation dominates and about 15 times higher than that due to $m = 2$ trailing wave. It is trivial to see that by increasing the peak amplitude of A_1 by a factor of 2, we would increase dL_z/dt roughly by a factor of 4 (see Eq. [27]). While the peak strength of the torque due to $m = 1$ (seen in the range $4 - 6 R_d$) is a few times smaller than due to $m = 2$ (seen in $< 2 R_d$) (see Fig. 9), the crucial point is that in the outer parts, it is the $m = 1$ perturbation that provides the channel that leads to the outward AMT.

6 DISCUSSION

1. Relative roles of $m = 1$ and $m = 2$ in AMT

The structure of a spiral galaxy is such that the inner region is dominated either by a bar and/or spiral arms and generally the outer part is dominated by lopsided asymmetry. There might be a deeper reason for such a configuration to exist in nature. Following Lynden-Bell & Kalnajs (1972), and a large amount of research by a number of authors (Tremaine & Weinberg 1984; Weinberg 1985;

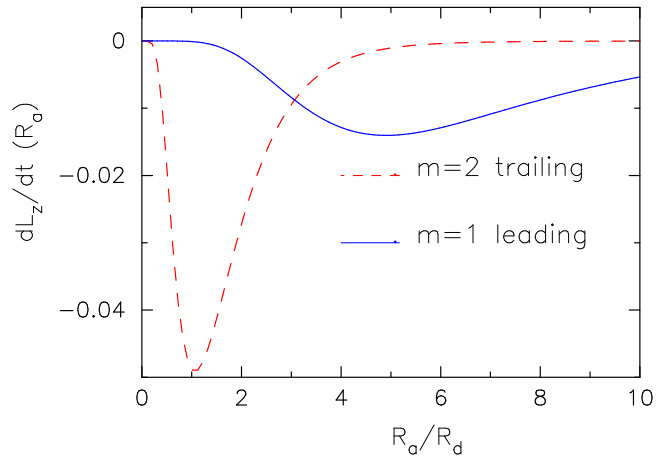


Figure 9. The plot showing the radial variation of the total torque (sum of gravity and advective) i.e., the net rate of change of angular momentum due to $m = 1$ and $m = 2$ perturbations for stars+gas+dark matter halo ($\rho_0 = 0.035 M_\odot pc^{-3}$). Note that only $m = 1$ leading perturbation can transport angular momentum outward (i.e., the disc with R_a loses angular momentum) opposite to the $m = 2$ perturbation which has to be trailing to do so. The unit of dL_z/dt is given by GM_d^2/R_d .

Hernquist & Weinberg 1992; Zhang 1999; Weinberg & Katz 2002; Athanassoula 2002, 2003; Sellwood & Debattista 2006; Dubinski et al. 2009; Saha et al. 2010, 2012), the important role played by a bar and spiral arms in galaxies has now been understood. Both a bar and spiral arms help in evolving an initially axisymmetric disc galaxy by redistributing energy and angular momentum so that the disc reaches a state of minimum energy configuration. The end product of this process is a growing central concentration or a pseudo-bulge formation (Combes & Sanders 1981; Pfenniger & Norman 1990; Raha et al. 1991; Kormendy & Kennicutt 2004; Saha & Naab 2013).

However, often this process requires gas to flow inwards. Plenty of observations suggest that galaxy accretes gas from outside either as a smooth infall - as shown by extended gas filaments as in NGC 891 (Mapelli et al. 2008), or via satellites (e.g., Zaritsky & Rix 1997), also see the recent review on gas accretion by Combes (2014). Numerical simulations also indicate that galaxies accrete gas along cosmological filaments (Kereš et al. 2005; Dekel et al. 2009). The importance of both $m = 1$ and $m = 2$ modes in driving gas inflow has been stressed previously by Combes (2001). But details about the angular momentum transport by $m = 1$ has not been worked out. As we understand now, unless there is a positive definite torque acting on the gas, it is hard for an inflow to occur in the first place or there has to be other mechanisms at work. We show that lopsidedness can act as a bridge between the stellar disc and the cosmic filaments which are a reservoir of cold gas. This galactic leading $m = 1$ mode is a machinery behind bringing gas to the edge of the stellar disc from where the gas inflow is taken care of by the spiral arms and bars. This is in compliance with the fact that the strength of lopsidedness decreases as one move inward towards the galactic center where generally $m = 2$ dominates.

We show using arguments similar to Lindblad, that on

kinematic grounds, the outer parts of an exponential disc are susceptible to an $m = 1$ mode. However, this has a transition point which marks the change of sign of AMT in the disc. This is removed if the disc is embedded in a dark matter halo so that the net κ dominates over Ω at all radii and an outward flow of angular momentum occurs smoothly at all radii, if the lopsided mode is leading. This gives a deeper meaning to the role played by the ubiquitous $m = 1$ modes in shaping or restructuring galaxies.

Thus, the $m = 1$ mode bridges the gap between the gas accretion from filaments onto the outer galaxy to transport to the inner galaxy. Inside the optical disc, the spiral arms take over as the main driver of AMT. Thus $m = 1$ in the outer parts and $m = 2$ in the inner parts together allow the secular galaxy evolution to proceed in a meaningful way. The $m = 1$ leading and $m = 2$ trailing modes can be thought of as collaborators in a relay process where the $m = 1$ mode facilitates gas infall up to about half the optical radius, inside of which the $m = 2$ takes over as the agent that allows gas infall. Thus together these modes cause an outward AMT and allow a smooth secular evolution of a typical galactic disc. This then is the deep physical reason for the existence of $m = 1$ mode, analogous to what Lynden-Bell (1979) had shown $m = 2$ to be a mechanism that structures spirals within the inner optical disc.

2. Discs in dark matter halo vs. Bare discs

Interestingly, the other typical disc mass distributions such Toomre's model $n = 2$ (as used e.g., by Bournaud et al. (2005) and others), and a Gaussian distribution as seen in the HI in some galaxies (Angiras et al. 2006; van Eymeren et al. 2011a) also require a dark matter halo to have a smooth flow of angular momentum (see the Appendix for details). Surprisingly, the power-law mass distributions that are often seen as bare systems as in pre-stellar regions (Lizano & Shu 1989) do not exhibit such a transition region and hence do not have a discontinuity in the outward AMT, which may explain why such bare systems can exist. Conversely, an exponential or a Gaussian radial mass distribution cannot exist as bare discs without the cushioning of a dark matter halo that removes the transition point.

7 CONCLUSIONS

In this paper, we have studied the angular momentum transport mediated by a slowly rotating lopsided asymmetry due to the standard or gravity torques as well as the lorry or advective torques. In particular, we work out the lorry transport of angular momentum in considerable detail to understand the role played by the ubiquitous lopsided perturbation in driving evolution in lopsided disk galaxies. Our main conclusions are the following:

We show that in the long-wave limit, the magnitude of advective torque due to a lopsided perturbation dominates over the gravity torque and opposes the angular momentum flow due to the gravity torque unlike the case of an $m = 2$ perturbation.

We show that in an exponential stellar disc with or without cold gas, there is a transition point at which a kinematic lopsided perturbation changes from retrograde to prograde. We show that there are other mass distributions e.g.,

Toomre's model n , Gaussian distribution, for which this is also true. It is shown that in the presence of a transition point, the net angular momentum flow due to a lopsided perturbation is hindered in such a mass distribution.

We then explicitly show that in the presence of a dark matter halo such a transition point is uplifted, allowing a smooth flow of angular momentum in the disc. In a typical lopsided galaxy, where an exponential disc is embedded in a dark matter halo, an outward smooth transport of angular momentum occurs only when the lopsidedness is leading in nature. This can facilitate smooth gas infall in the galaxy.

ACKNOWLEDGEMENT

The authors thank the anonymous referee for very constructive and insightful comments on the manuscript.

APPENDIX A: APPLICATION TO OTHER DENSITY DISTRIBUTION

A1 Toomre's model n

The surface density distribution for Toomre's model n is given by (Toomre 1963)

$$\Sigma_n(R) = \Sigma_0 \left(1 + \frac{R^2}{2nR_T^2}\right)^{-(n+1/2)}, \quad (\text{A1})$$

where R_T is the scale length and n an integer. Note that in the limit $n \rightarrow \infty$, the above density distribution becomes a Gaussian density distribution which we discuss separately in the next section. The potential for this disc model can be obtained using the Bessel function expansion approach as

$$\Phi_n(R, z) = \int_0^\infty S_n(k) J_0(kR) e^{-k|z|} dk, \quad (\text{A2})$$

where the function $S_n(k)$ is given by

$$S_n(k) = -2\pi G \int_0^\infty J_0(kR) \Sigma_n(R) R dR \quad (\text{A3})$$

Solving for the above integral, we have the potential for the Toomre's model n

$$\Phi_n(R, z) = -\Lambda_n \int_0^\infty k^{n-1/2} J_0(kR) K_{n-1/2}(\alpha_n k) e^{-k|z|} dk \quad (\text{A4})$$

In the above equation, $\Lambda_n = 4\pi G \Sigma_0 R_T^2 \frac{n}{\Gamma(n+1/2)} (\alpha_n/2)^{n-1/2}$, $\alpha_n = 2nR_T^2$ and $K_{n-1/2}$ denotes the modified Bessel function of 2nd order.

The azimuthal frequency for the disc can be derived using the following equation:

$$\Omega_n^2(R) = \Lambda_n \frac{2^n \Gamma(3/2) \Gamma(n+1)}{\sqrt{2} \alpha_n^{n+5/2}} F\left[n+1, \frac{3}{2}; 2; -\frac{R^2}{\alpha_n^2}\right] \quad (\text{A5})$$

The ratio of radial epicyclic (κ) to azimuthal frequency can be obtained using the following analytic expression:

$$\frac{\kappa_n^2}{\Omega_n^2} = 2 \left[1 + \frac{F\left[n+1, \frac{3}{2}, 1; -\frac{R^2}{\alpha_n^2}\right]}{F\left[n+1, \frac{3}{2}, 2; -\frac{R^2}{\alpha_n^2}\right]} \right], \quad (\text{A6})$$

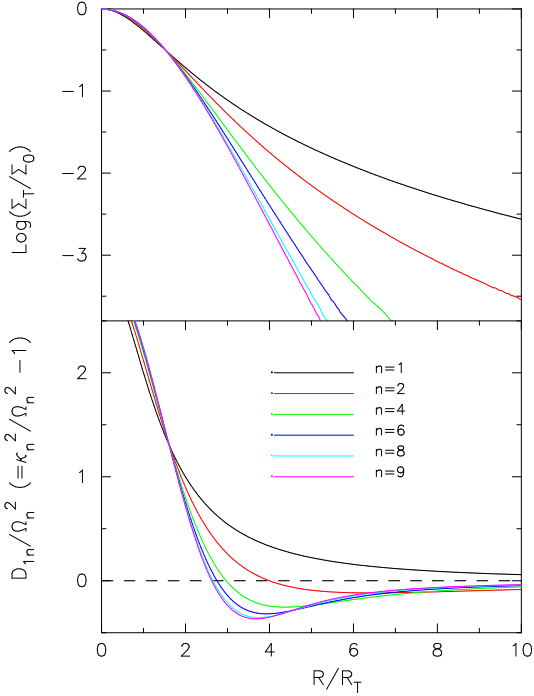


Figure A1. Surface density distribution and the corresponding D_1 parameter for the family of Toomre's model n . For $n=1$, it is actually the Kuzmin disc.

where the functions F refer to the hypergeometric function. The D_1 parameter for the family of models are trivially given by

$$\frac{D_{1n}}{\Omega_n^2} = \frac{\kappa_n^2}{\Omega_n^2} - 1 \quad (\text{A7})$$

In Fig. A1, we show the surface density variation and the corresponding profiles of D_{1n} . It is clear that all $n \geq 2$ Toomre's models n have $\kappa/\Omega < 1$, or $D_{1n} < 0$, in some radial range. For higher n models, the values of transition radii R_{tr} decrease; although for really high $n > 8$, R_{tr} does not change appreciably. For $n = 1$ Toomre model, there is no transition point so there is a smooth outward AMT.

A2 Gaussian density distribution

The surface density of a Gaussian disc is given by

$$\Sigma_g(R) = \Sigma_{g0} e^{-R^2/2R_g^2} \quad (\text{A8})$$

Again we determine the potential using the Bessel function approach outlined above:

$$\Psi_g(R, z=0) = -2\pi G \int_0^\infty dk J_0(kR) \int_0^\infty dR' R' J_0(kR') \Sigma_g(R'), \quad (\text{A9})$$

Solving this integral the potential for the disc distribution can be obtained as

$$\Psi_g(R, z=0) = -\sqrt{2\pi} \pi G \Sigma_{g0} R_g e^{-y_g^2} I_0(y_g^2), \quad (\text{A10})$$

where $y_g = R/2R_g$.

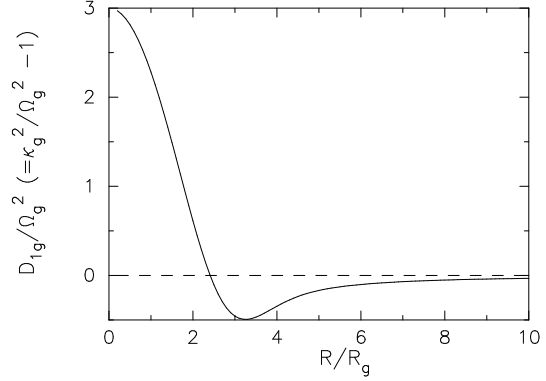


Figure A2. Radial variation of the D_{1g} parameter for the Gaussian disc.

It is then straightforward to derive the circular frequency in such a disc and is given by

$$\Omega_g^2(R) = \sqrt{\frac{\pi}{2}} \frac{\pi G \Sigma_{g0}}{R_g} e^{-y_g^2} [I_0(y_g^2) - I_1(y_g^2)] \quad (\text{A11})$$

The ratio of κ/Ω for the Gaussian disc can be obtained from this formula:

$$\frac{\kappa_g^2}{\Omega_g^2} = 4 - \left[4y_g^2 - \frac{2I_1(y_g^2)}{I_0(y_g^2) - I_1(y_g^2)} \right] \quad (\text{A12})$$

In Fig. A2, we show the radial variation of $\frac{D_{1g}}{\Omega_g^2} = \frac{\kappa_g^2}{\Omega_g^2} - 1$. The transition radius for this disc arises at $R = 2.42R_g$.

A3 Power law disc

We consider the surface density distribution of a power law disc as

$$\Sigma_p(R) = \Sigma_{p0} \left(\frac{R}{R_0}\right)^{-p} \quad (\text{A13})$$

Using the Bessel function expansion approach as done in previous section, we have the potential for a razor thin power law disc:

$$\Phi_p(R, z) = -2\pi G \Sigma_{p0} R_0^p 2^{-(p-1)} \frac{\Gamma(1-p/2)}{\Gamma(p/2)} \int_0^\infty k^{p-2} J_0(kR) e^{-k|z|} dk \quad (\text{A14})$$

Which when computed at $z = 0$ is given by

$$\Phi_p(R, 0) = -\pi G \Sigma_{p0} R_0 K(p) (R/R_0)^{-(p-1)}, \quad (\text{A15})$$

where the function $K(p)$ is

$$K(p) = \frac{\Gamma[1-p/2]\Gamma[(p-1)/2]}{\Gamma[(3-p)/2]\Gamma[p/2]} \quad (\text{A16})$$

The allowed range for the power law exponent is $1 < p < 5/2$.

The circular frequency is given by

$$\Omega_p^2(R) = \pi G \Sigma_{p0} R_0^p (p-1) K(p) R^{-(p+1)} \quad (\text{A17})$$

The ratio κ/Ω for the power law discs turns out to be independent of radius r and simply depends on the power law index:

$$\frac{\kappa^2}{\Omega^2} = 3 - p; \quad 1 < p < 5/2 \quad (\text{A18})$$

Thus, $\kappa/\Omega > 1$ for $p \leq 2$, hence there is no transition point, thus there is a smooth flow of angular momentum at all radii.

REFERENCES

- Angiras R. A., Jog C. J., Dwarakanath K. S., Verheijen M. A. W., 2007, *MNRAS*, 378, 276
- Angiras R. A., Jog C. J., Omar A., Dwarakanath K. S., 2006, *MNRAS*, 369, 1849
- Athanassoula E., 2002, *ApJL*, 569, L83
- Athanassoula E., 2003, *MNRAS*, 341, 1179
- Athanassoula E., Misiriotis A., 2002, *MNRAS*, 330, 35
- Baldwin J. E., Lynden-Bell D., Sancisi R., 1980, *MNRAS*, 193, 313
- Bigiel F., Blitz L., 2012, *ApJ*, 756, 183
- Binney J., Merrifield M., 1998, *Galactic Astronomy*
- Binney J., Tremaine S., 1987, *Galactic dynamics*
- Binney J., Tremaine S., 2008, *Galactic Dynamics: Second Edition*. Princeton University Press
- Block D. L., Bertin G., Stockton A., Grosbol P., Moorwood A. F. M., Peletier R. F., 1994, *A&A*, 288, 365
- Bournaud F., Combes F., Jog C. J., Puerari I., 2005, *A&A*, 438, 507
- Brand J., Blitz L., 1993, *A&A*, 275, 67
- Buta R. J., Byrd G. G., Freeman T., 2003, *AJ*, 125, 634
- Combes F., 2001, in Aretxaga I., Kunth D., Mújica R., eds, *Advanced Lectures on the Starburst-AGN Fueling the AGN*. p. 223
- Combes F., 2014, in Seigar M. S., Treuhardt P., eds, *Astronomical Society of the Pacific Conference Series Vol. 480 of Astronomical Society of the Pacific Conference Series, Gas Accretion in Disk Galaxies*. p. 211
- Combes F., Debbasch F., Friedli D., Pfenniger D., 1990, *A&A*, 233, 82
- Combes F., Sanders R. H., 1981, *A&A*, 96, 164
- Combes et al. 2014, *A&A*, 565, A97
- Considera S., Athanassoula E., 1982, *A&A*, 111, 28
- de Zeeuw T., Pfenniger D., 1988, *MNRAS*, 235, 949
- Debattista V. P., Carollo C. M., Mayer L., Moore B., 2004, *ApJL*, 604, L93
- Dekel A., Birnboim Y., Engel G., Freundlich J., Goerdt T., Mumcuoglu M., Neistein E., Pichon C., Teyssier R., Zinger E., 2009, *Nature*, 457, 451
- Dubinski J., Berentzen I., Shlosman I., 2009, *ApJ*, 697, 293
- Durbala A., Buta R., Sulentic J. W., Verdes-Montenegro L., 2009, *MNRAS*, 397, 1756
- Dury V., de Rijcke S., Debattista V. P., Dejonghe H., 2008, *MNRAS*, 387, 2
- Earn D. J. D., Lynden-Bell D., 1996, *MNRAS*, 278, 395
- Freeman K. C., 1970, *ApJ*, 160, 811
- Goldreich P., Tremaine S., 1979, *ApJ*, 233, 857
- Grouchy R. D., Buta R., Salo H., Laurikainen E., Speltincx T., 2008, *AJ*, 136, 980
- Hernquist L., Weinberg M. D., 1992, *ApJ*, 400, 80
- Hunter C., 1979, *ApJ*, 227, 73
- Jog C. J., 1996, *MNRAS*, 278, 209
- Jog C. J., 1997, *ApJ*, 488, 642
- Jog C. J., 1999, *ApJ*, 522, 661
- Jog C. J., 2000, *ApJ*, 542, 216
- Jog C. J., 2011, *Memorie della Societa Astronomica Italiana Supplementi*, 18, 119
- Jog C. J., 2014, *AJ*, 147, 132
- Jog C. J., Combes F., 2009, *Physics Reports*, 471, 75
- Kereš D., Katz N., Weinberg D. H., Davé R., 2005, *MNRAS*, 363, 2
- Kikuchi N., Korchagin V., Miyama S. M., 1997, *ApJ*, 478, 446
- Kormendy J., 2008, in Bureau M., Athanassoula E., Barbuy B., eds, *IAU Symposium Vol. 245 of IAU Symposium, Internal secular evolution in disk galaxies: the growth of pseudobulges*. pp 107–112
- Kormendy J., Kennicutt Jr. R. C., 2004, *ARA&A*, 42, 603
- Laurikainen E., Salo H., Buta R., Knapen J. H., 2007, *MNRAS*, 381, 401
- Lewis B. M., 1984, *ApJ*, 285, 453
- Lizano S., Shu F. H., 1989, *ApJ*, 342, 834
- Lynden-Bell D., 1979, *MNRAS*, 187, 101
- Lynden-Bell D., Kalnajs A. J., 1972, *MNRAS*, 157, 1
- Malhotra S., 1995, *ApJ*, 448, 138
- Mapelli M., Moore B., Bland-Hawthorn J., 2008, *MNRAS*, 388, 697
- Ostriker J. P., Peebles P. J. E., 1973, *ApJ*, 186, 467
- Pasha I. I., Tsitsin F. A., 1979, *Soviet Astronomy Letters*, 5, 335
- Pfenniger D., Norman C., 1990, *ApJ*, 363, 391
- Raha N., Sellwood J. A., James R. A., Kahn F. D., 1991, *Nature*, 352, 411
- Richter O.-G., Sancisi R., 1994, *A&A*, 290, L9
- Rix H.-W., Zaritsky D., 1995, *ApJ*, 447, 82
- Saha K., Combes F., Jog C. J., 2007, *MNRAS*, 382, 419
- Saha K., Levine E. S., Jog C. J., Blitz L., 2009, *ApJ*, 697, 2015
- Saha K., Martinez-Valpuesta I., Gerhard O., 2012, *MNRAS*, 421, 333
- Saha K., Naab T., 2013, *MNRAS*, 434, 1287
- Saha K., Tseng Y., Taam R. E., 2010, *ApJ*, 721, 1878
- Sellwood J. A., Debattista V. P., 2006, *ApJ*, 639, 868
- Spitzer L., 1978, *Physical processes in the interstellar medium*
- Toomre A., 1963, *ApJ*, 138, 385
- Toomre A., 1981, in S. M. Fall & D. Lynden-Bell ed., *Structure and Evolution of Normal Galaxies What amplifies the spirals*. pp 111–136
- Tremaine S., Weinberg M. D., 1984, *MNRAS*, 209, 729
- van Eymeren J., Jütte E., Jog C. J., Stein Y., Dettmar R.-J., 2011a, *A&A*, 530, A29
- van Eymeren J., Jütte E., Jog C. J., Stein Y., Dettmar R.-J., 2011b, *A&A*, 530, A30
- Weinberg M. D., 1985, *MNRAS*, 213, 451
- Weinberg M. D., Katz N., 2002, *ApJ*, 580, 627
- Wilcots E. M., Prescott M. K. M., 2004, *AJ*, 127, 1900
- Zaritsky D., Rix H.-W., 1997, *ApJ*, 477, 118
- Zaritsky et al. D., 2013, *ApJ*, 772, 135
- Zhang X., 1999, *ApJ*, 518, 613